Dalton Transactions

PAPER

Homo- and heteropolymetallic 3-(2-pyridyl)-pyrazolate manganese and rhenium complexes†

Cite this: DOI: 10.1039/c3dt53439a

Marta Arroyo,[a] Patricia Gómez-Iglesias,[a] Noelia Antón,[a] Raúl García-Rodríguez,[a] Elisabete C. B. A. Alegria,[b,c] Armando J. L. Pombeiro,[b] Daniel Miguel[a] and Fernando Villafañe*[a]

fac-[MBr(CO)$_3$(pypzH)] (M = Mn, Re; pypzH = (3-(2-pyridyl)pyrazole) complexes are prepared from *fac*-[MBr(CO)$_3$(NCMe)$_2$] and pypzH. The result of their deprotonation depends on the metallic substrate: the rhenium complex affords cleanly the bimetallic compound [*fac*-{Re(CO)$_3$(μ^2-pypz)}]$_2$ (μ^2-pypz = μ^2-3-(2-pyridyl-κ^1N)pyrazolate-2κ^1N), which was crystallographically characterized, whereas a similar manganese complex was not detected. When two equivalents of pyridylpyrazolate are used, polymetallic species [*fac*-M(CO)$_3$(μ^2-pypz)(μ^3-pypz)M′] (μ^3-pypz = μ^3-3-(2-pyridyl-κ^1N)pyrazolate-1κ^2N,*N*:2κ^1N:; M = Mn, M′ = Li, Na, K; M = Re, M′ = Na) are obtained. The crystal structures of the manganese carbonylate complexes were determined. The lithium complex is a monomer containing one manganese and one lithium atom, whereas the sodium and potassium complexes are dimers and reveal an unprecedented coordination mode for the bridging 3-(2-pyridyl)pyrazolate ligand, where the nitrogen of the pyridyl fragment and the nitrogen-1 of pyrazolate are chelated to manganese atoms, and each nitrogen-2 of pyrazolate is coordinated to two alkaline atoms. The polymetallic carbonylate complexes are unstable in solution and evolve spontaneously to [*fac*-{Re(CO)$_3$(μ^2-pypz)}]$_2$ or to the trimetallic paramagnetic species [Mn^{II}(μ^2-pypz)$_2${*fac*-{Mn^{I}(CO)$_3$(μ^2-pypz)}$_2$}]. The related complex *cis*-[MnCl$_2$(pypzH)$_2$] was also synthesized and structurally characterized. The electrochemical behavior of the new homo- and heteropolymetallic 3-(2-pyridyl)pyrazolate complexes has been studied and details of their redox properties are reported.

Received 6th December 2013,
Accepted 24th December 2013

DOI: 10.1039/c3dt53439a

www.rsc.org/dalton

Introduction

The 3-(2-pyridyl)pyrazole (pypzH) ligand has been extensively used as a bidentate ligand similar to 2,2′-bipyridyl (Fig. 1a), and its complexes have found a wide variety of applications, from catalysis[1] to photophysical properties,[2] information processing or host–guest chemistry.[3] The first complex containing bridging 3-(2-pyridyl)pyrazolate after deprotonation and coordination to a second metallic center (Fig. 1b) was obtained in 1996,[4] and since then a broad diversity of examples of this type of homopolymetallic complexes have been described.[3–5] In contrast, there seems to be only a couple of examples of heterobimetallic complexes (Fig. 1c), although they present promising features, such as the self-assembly of supramolecules with helical structures or the design of "light-controlled ion switches".[6]

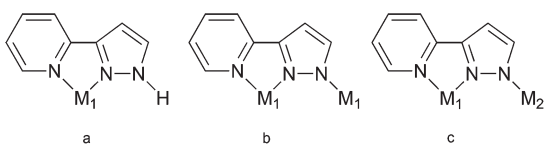

Fig. 1 3-(2-Pyridyl)pyrazole and 3-(2-pyridyl)pyrazolate coordination modes.

As part of our studies on the chemistry of group 7 pyrazolylamidino complexes,[7] we decided to explore the coordination of the 3-(2-pyridyl)pyrazole ligand to these metals. A similar study on group 6 metals has given rise to new bimetallic allyldicarbonylmolybdenum(II) complexes with a marked connection between both metallic centres through the bridging pyridylpyrazolates.[8] Herein we study their synthesis and reactivity towards bases, which has allowed us to obtain new polymetallic homo- and heteronuclear 3-(2-pyridyl)pyrazolate complexes. Polynuclear manganese complexes in various oxidation states are gaining interest due to their novel magnetic

[a]GIR MIOMeT-IU Cinquima-Química Inorgánica, Facultad de Ciencias, Campus Miguel Delibes, Universidad de Valladolid, 47011 Valladolid, Spain
[b]Centro de Química Estrutural, Complexo I, Instituto Superior Técnico, Universidade de Lisboa, 1049-001 Lisboa, Portugal
[c]Química Chemical Engeneering Departmental Area, ISEL, R. Conselheiro Emídio Navarro, 1959-007 Lisboa, Portugal

†CCDC 873520, 974910, 873521, 974911, 873522 and 873523. For crystallographic data in CIF or other electronic format see DOI: 10.1039/c3dt53439a

properties, related to the single-molecule-magnetic behavior and associated quantum properties.[9]

Results and discussion

Synthesis and characterization of the Mn(I) and Re(I) complexes

The complexes *fac*-[MBr(CO)$_3$(pypzH)], M = Mn (**1a**), Re (**1b**), were prepared in high yield from the reactions of *fac*-[MBr(CO)$_3$(NCMe)$_2$] with pypzH in a 1 : 1 ratio, and were analytically and spectroscopically characterized (see the Experimental section).

As indicated above, the deprotonation of a pypzH ligand may lead to obtainment of polymetallic complexes; therefore **1a** and **1b** were treated with a MeOH solution of NaOMe.

When using the manganese complex **1a**, the expected bimetallic complex, coming from the deprotonation of pypzH and elimination of the bromido ligand, giving a bridging 3-(2-pyridyl)pyrazolate, could not be detected in solution. This is the expected result of this process, and in fact it is produced when the rhenium complex **1b** is used as the starting material (*vide infra*). However, for manganese the reaction mixture evolves to the tetrametallic complex [{*fac*-Mn(CO)$_3$(μ^2-pypz)(μ^3-pypz)Na}$_2$], Na-**3a** (Scheme 1), which could be crystallographically characterized (Fig. 2 and Table 1). Although the Mn/pypzH ratio used is 1/1, in Na-**3a** the Mn/pypzH ratio is 1/2; therefore it is a decomposition product. Thus, Na-**3a** was synthesized selectively by treating *fac*-[MnBr(CO)$_3$(NCMe)$_2$] with two equivalents of sodium pyridylpyrazolate, which afforded Na-**3a** in a 73% yield (Scheme 1).

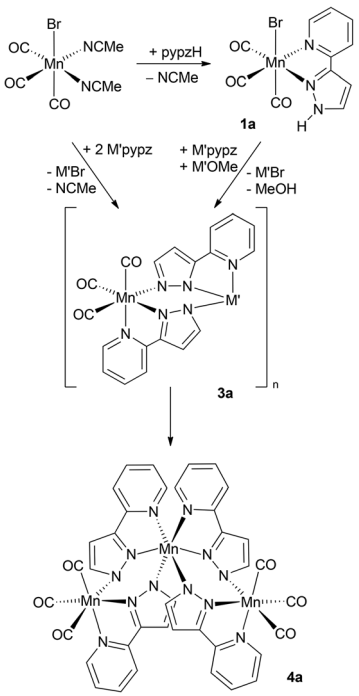

Scheme 1

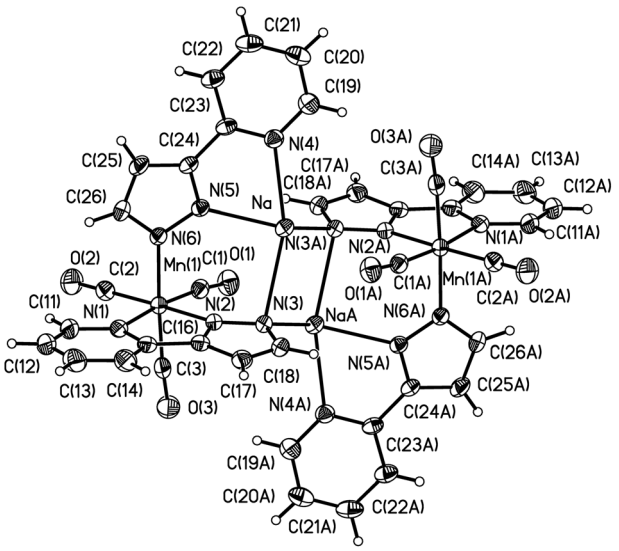

Fig. 2 Perspective view of [{*fac*-Mn(CO)$_3$(μ^2-pypz)(μ^3-pypz)Na}$_2$], Na-**3a**, showing the atom numbering. Ellipsoids are drawn at 30% probability.

The crystal structure of Na-**3a** was shown to be a dimer of the monomer "*fac*-Mn^{I}(CO)$_3$(μ^2-pypz)(μ^3-pypz)Na". There are two different types of bridging pyridylpyrazolate: one is chelating sodium and the second is chelating manganese. The first one adopts the expected heterobimetallic bridging coordination mode, that is, that shown in Fig. 1c. Surprisingly, in the bridging pyridylpyrazolate chelating manganese, the nitrogen previously protonated is not coordinated to one metal center, as usual, but to two metallic atoms, two sodiums in this case (IV in Fig. 3). We have not been able to find any precedent of this type of coordination where a pyridylpyrazolate is bridging to three metals, which contrasts with that usually found, bridging to two metals (III in Fig. 3). Similar bridging of pyrazolate to three metals (II in Fig. 3) has already been described.[10] It should be noted that this type of bridging is indicative of some type of electronic deficiency. Sodiums are bonded to a chelating pyridylpyrazolate ligand, and to two pyrazolyl moieties, whereas a non-bonding interaction with the nearby oxygen atom of one carbonyl completes the 5-coordinated environment. The coordination of sodium to a pyridylpyrazolate is also unprecedented. There is a report on bridging pyrazolates in a manganese–sodium polymetallic complex, where the Na–N distances are similar to those found in Na-**3a**.[11] The aromatic rings in the pyridylpyrazolate are not coplanar, the dihedral angles being 6° for those chelating manganese and 13° for those chelating sodium.

The formation of Na-**3a** leads us to consider whether this unexpected tetranuclear structure is the result of a sodium template effect, and therefore to determine whether similar results might be obtained by using (a) other alkali metal ions and (b) rhenium instead of manganese.

The second point is discussed below. In order to answer the first of these points, similar reactions were carried out treating

Table 1 Selected distances (Å) and angles (°) for [*fac*-Mn(CO)$_3$(pypz)-(μ^2-pypz)Li(OH$_2$)(THF)], Li-**3a**, [{*fac*-Mn(CO)$_3$(μ^2-pypz)(μ^3-pypz)Na}$_2$], Na-**3a**, and [{*fac*-Mn(CO)$_3$(μ^2-pypz)(μ^3-pypz)K(THF)}$_2$], K-**3a**

	Li-**3a**	Na-**3a**	K-**3a**
Mn(1)–C(1)	1.795(4)	1.774(3)	1.807(12)
Mn(1)–C(2)	1.805(4)	1.811(3)	1.782(10)
Mn(1)–C(3)	1.788(4)	1.793(3)	1.766(13)
Mn(1)–N(1)	2.082(3)	2.075(2)	2.059(8)
Mn(1)–N(2)	2.002(3)	2.010(2)	2.009(7)
Mn(1)–N(6)	2.051(3)	2.038(2)	2.037(8)
C(1)–O(1)	1.141(4)	1.157(3)	1.141(11)
C(2)–O(2)	1.133(4)	1.141(3)	1.163(10)
C(3)–O(3)	1.140(4)	1.140(3)	1.138(11)
N(3)–M′		2.657(2)	2.857(8)
N(3A)–M′		2.439(2)	2.823(9)
N(4)–M′	2.090(7)	2.461(2)	2.789(10)
N(5)–M′	2.030(7)	2.329(2)	2.709(8)
M′–O(1A)		2.890(3)	3.249(9)
Li–O(50)	1.864(8)		
M′–O(40)	1.982(8)		2.789(9)
C(1)–Mn(1)–C(2)	91.78(16)	91.22(12)	90.0(4)
C(1)–Mn(1)–C(3)	88.90(17)	86.66(13)	89.9(5)
C(2)–Mn(1)–C(3)	88.26(19)	92.96(13)	90.2(5)
C(1)–Mn(1)–N(1)	171.81(15)	172.32(10)	170.3(3)
C(2)–Mn(1)–N(1)	95.01(15)	96.21(11)	98.1(4)
C(3)–Mn(1)–N(1)	95.88(14)	91.03(13)	95.4(4)
C(1)–Mn(1)–N(2)	95.08(14)	94.06(10)	94.5(4)
C(2)–Mn(1)–N(2)	173.11(14)	174.65(11)	175.5(4)
C(3)–Mn(1)–N(2)	91.26(16)	88.16(11)	89.0(4)
C(1)–Mn(1)–N(6)	89.64(13)	94.55(10)	94.5(4)
C(2)–Mn(1)–N(6)	91.35(14)	91.61(10)	90.5(4)
C(3)–Mn(1)–N(6)	178.48(14)	175.25(12)	178.9(4)
N(1)–Mn(1)–N(2)	78.20(12)	78.53(8)	77.5(3)
N(1)–Mn(1)–N(6)	85.62(10)	87.18(8)	85.3(3)
N(6)–Mn(1)–N(2)	89.30(11)	87.17(8)	90.4(3)
N(4)–M′–N(3)		156.54(8)	146.1(3)
N(5)–M′–N(4)	82.4(3)	71.17(7)	63.0(3)
N(5)–M′–N(3A)		119.20(8)	106.6(2)
N(3A)–M′–N(4)		103.43(8)	96.6(3)
N(5)–M′–N(3)		91.52(7)	83.8(2)
N(3)–M′–N(3A)		98.80(7)	85.7(2)
M′–N(3)–M′(A)		81.20(7)	94.3(2)
N(4)–Li–O(40)	98.6(3)		
N(4)–Li–O(50)	120.9(4)		
N(5)–Li–O(40)	118.1(4)		
N(5)–Li–O(50)	118.1(4)		

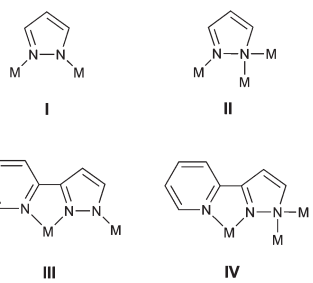

Fig. 3 Pyrazolate and 3-(2-pyridyl)pyrazolate coordination modes.

1a with LiOMe or KOMe, which afforded Li-**3a** and K-**3a** in 70% and 76% yields respectively (Scheme 1). Both could be crystallographically characterized (Fig. 4 and Table 1).[12] The structure of K-**3a** is discussed first, given its analogy with that of Na-**3a**.

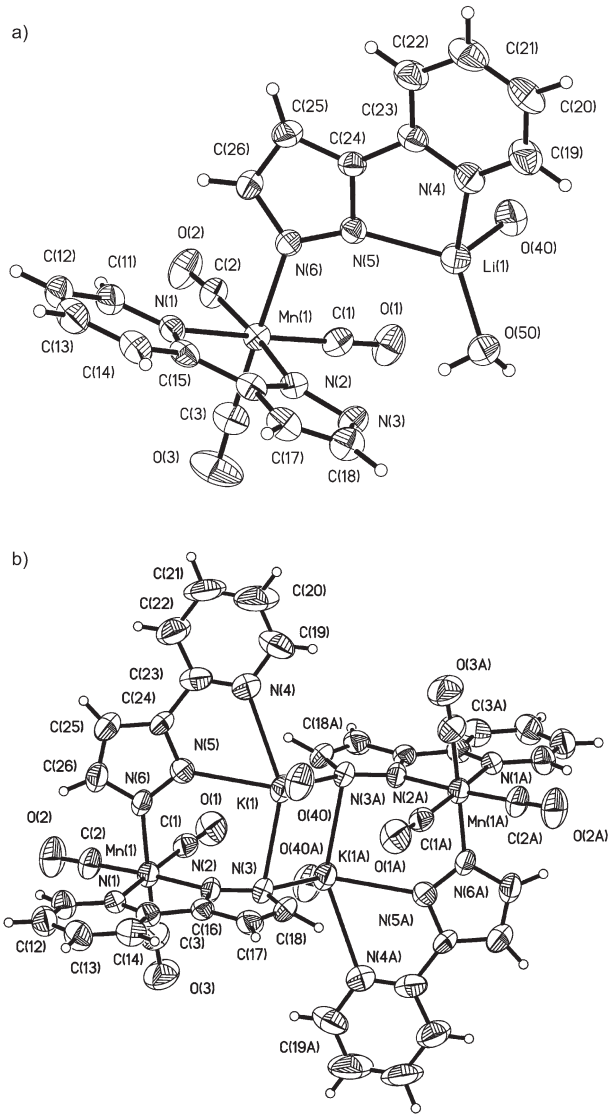

Fig. 4 Perspective views of [*fac*-Mn(CO)$_3$(pypz)(μ^2-pypz)Li(OH$_2$)(THF)], Li-**3a**, and [{*fac*-Mn(CO)$_3$(μ^2-pypz)(μ^3-pypz)K(THF)}$_2$], K-**3a**, showing the atom numbering. Ellipsoids are drawn at 30% probability. Only the oxygen donor atoms of the coordinated THF molecules are shown (O40); their hydrocarbon chains have been omitted for clarity.

The crystal structure of K-**3a** (Fig. 4, bottom) is also a dimer of the monomer "*fac*-Mn^{I}(CO)$_3$(μ^2-pypz)(μ^3-pypz)K", and again two different types of bridging pyridylpyrazolate (chelating sodium and chelating manganese) are found. As for Na-**3a**, the nitrogen previously protonated of the second is coordinated to two potassiums (IV in Fig. 3). Opposite to Na-**3a** where the fifth coordination position of sodium was occupied by an oxygen atom of one of the carbonyls, in K-**3a** an oxygen atom of a THF molecule is coordinated to potassium, whereas the oxygen of the nearest carbonyl is at 3.249(9) Å, too far to consider any interaction. As expected, the distances and angles of the manganese fragment are quite similar in both structures, whereas those where the alkali atom is involved are larger for K-**3a** (Table 1). The dihedral angles of the aromatic rings in the

pyridylpyrazolate (5° for those chelating manganese and 12° for those chelating sodium) are also very similar to those found for Na-**3a**.

The crystal structure of Li-**3a** (Fig. 4, up) is a monomer, where the pyridylpyrazolate chelating manganese is only coordinated to manganese and therefore is not a bridging ligand. This is very surprising for a chelating pyridylpyrazolate, as we have found only one precedent in the literature of this type of coordination.[13] The pyridylpyrazolate chelating to lithium is a "typical" bridging pyridylpyrazolate (III in Fig. 3). The lithium coordination is a distorted tetrahedron where the other two coordination positions are occupied by the oxygen atoms of a molecule of THF and of a molecule of water.[14] Again the distances and angles of the manganese fragment are quite similar to those found in the other structures above, whereas those where the alkali atom is involved are shorter for Li-**3a** (Table 1). Again the aromatic rings in the pyridylpyrazolate are not coplanar; in this case both dihedral angles are similar (5° for that chelating manganese and 6° for that chelating lithium). The higher coplanarity of the rings in the bridging pyridylpyrazolate chelating lithium might be related to the lower steric requirements of the molecule.

The size of the alkali metal atoms allows an immediate interpretation of the crystal structures of the Li, Na and K salts of **3a**. Thus, the smaller lithium is tetracoordinated by both nitrogen atoms of a chelating pyridylpyrazolate and by two oxygen atoms of THF and water. However, sodium and potassium require a fifth donor atom to achieve pentacoordination. For sodium, a short contact with an oxygen atom of one of the carbonyls of the molecule seems to be enough to stabilize the structure, whereas the larger potassium requires the coordination of a more steric demanding molecule of THF. We have found very scarce reports on comparative structural studies of alkali metal compounds.[15]

For rhenium, the result of the deprotonation of the pypzH complex **1b** when treated with a MeOH solution of NaOMe is straightforward. In this case the product was the binuclear complex [*fac*-{Re(CO)$_3$(μ^2-pypz)}]$_2$, **2b** (Scheme 2), as a result of

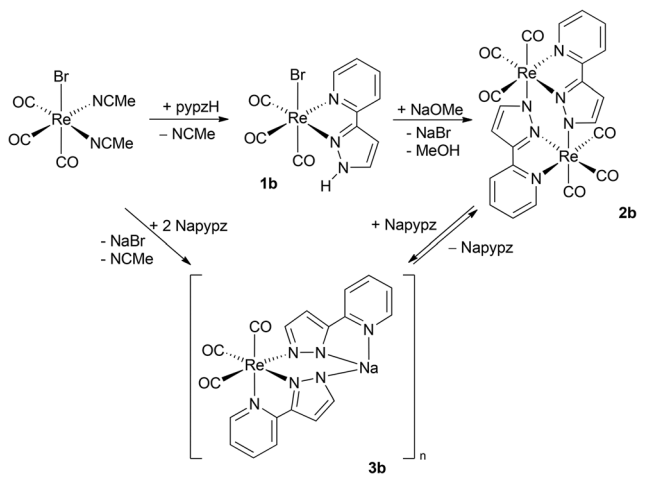

Scheme 2

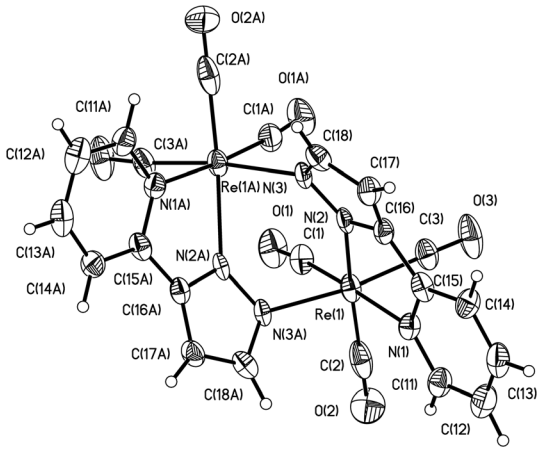

Fig. 5 Perspective view of [*fac*-{Re(CO)$_3$(μ^2-pypz)}]$_2$, **2b**, showing the atom numbering. Ellipsoids are drawn at 30% probability.

Table 2 Selected distances (Å) and angles (°) for [*fac*-{Re(CO)$_3$-(μ^2-pypz)}]$_2$, **2b**

Re(1)–C(1)	1.931(13)
Re(1)–C(2)	1.87(2)
Re(1)–C(3)	1.917(12)
Re(1)–N(1)	2.227(9)
Re(1)–N(2)	2.217(9)
Re(1)–N(3A)	2.149(8)
C(1)–O(1)	1.147(13)
C(2)–O(2)	1.198(18)
C(3)–O(3)	1.143(13)
C(1)–Re(1)–C(2)	82.1(5)
C(1)–Re(1)–C(3)	91.4(5)
C(2)–Re(1)–C(3)	88.5(6)
C(1)–Re(1)–N(1)	176.1(5)
C(2)–Re(1)–N(1)	94.1(5)
C(3)–Re(1)–N(1)	87.9(4)
C(1)–Re(1)–N(2)	111.5(4)
C(2)–Re(1)–N(2)	165.3(4)
C(3)–Re(1)–N(2)	96.4(4)
C(1)–Re(1)–N(3A)	86.9(4)
C(2)–Re(1)–N(3A)	98.8(5)
C(3)–Re(1)–N(3A)	172.2(5)
N(2)–Re(1)–N(3A)	77.2(3)
N(1)–Re(1)–N(2)	72.4(3)
N(1)–Re(1)–N(3A)	94.3(3)

the deprotonation of pypzH, which occurs with elimination of the bromido ligand, so the 3-(2-pyridyl)pyrazolate coordinates as a bridging ligand. Compound **2b** could be crystallographically characterized (Fig. 5 and Table 2).

The molecule is centrosymmetric and contains two "*fac*-[Re(CO)$_3$(pypz)]" moieties, where the "sixth" coordination position is occupied by the deprotonated nitrogen of the pyrazole, which chelates to the other rhenium atom. The octahedral geometry around the metal centers is clearly distorted, as shown by the *trans* [C(1)–Re(1)–N(1) 176.1(5); C(2)–Re(1)–N(2) 165.3(4); C(3)–Re(1)–N(3A) 172.2(5)] and *cis* OC–Re–N (from 72.4(3)° to 111.5(4)°) angles. The pyrazolate and pyridyl rings are not coplanar, their dihedral angle being 20°. The distances

and angles are similar to those found in the bimetallic rhenium complex [{(Re(CO)$_3$}$_2$TPP] where TPP = *meso*-tetraphenilporphyrine.[16] The distance between both rhenium atoms (3.977 Å) is too long to consider any interaction between them. An electrochemical study was carried out on **2b** (*vide infra*) in order to determine whether both metallic atoms may be connected by any electronic interaction.

As indicated above, the second point to consider after the formation of the sodium–manganese heterometallic compound Na-**3a** was whether rhenium could afford similar species. The deprotonation of the rhenium complex **1b** led cleanly to the expected dinuclear complex **2b**, whereas the similar reaction with manganese did not afford the corresponding bimetallic complex, which was not detected, but the heteronuclear complexes **3a**, where the Mn/pypz ratio is 1/2.[17] This led us to explore the behavior of the [*fac*-Re(CO)$_3$]$^+$ moiety when treated with two equivalents of Napypz. This reaction afforded a complex similar to **3a**, which is tentatively formulated as [{*fac*-Re(CO)$_3$(μ^2-pypz)(μ-pypz)Na}$_n$], **3b** (Scheme 2), since we were unable to obtain suitable monocrystals to perform an X-ray diffraction study. However, all the spectroscopic data are very similar to those of complexes **3a**, and analytical data (see the Experimental section) also support this proposal.

Synthesis and characterization of the Mn(II) complexes

The attempts to obtain crystals from the solutions of **3b** were complicated by its tendency to afford again **2b**, by the loss of one equivalent of Napypz (Scheme 2). Instead, the solutions of Na-**3a** evolve into the trimetallic complex [Mn^{II}(μ^2-pypz)$_2${*fac*-{Mn^{I}(CO)$_3$(μ^2-pypz)}$_2$}], **4a**, probably due to the presence of traces of oxygen, as one of the manganese atoms in this molecule is formally Mn(II) (Scheme 1). A selective synthesis of **4a** was attempted by treating Na-**3a** with different sources of Mn(II) such as Mn(BF$_4$)$_2$ or MnCl$_2$, but these reactions afforded complex mixtures which could not be characterized. The paramagnetism of **4a** precluded its characterization by NMR. Fortunately it crystallized as yellow needles and an X-ray determination could be carried out (Fig. 6, Table 3).[18]

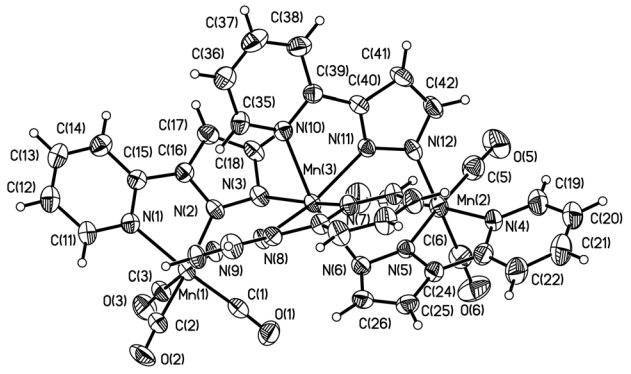

Fig. 6 Perspective view of [Mn(μ^2-pypz)$_2${*fac*-{Mn(CO)$_3$(μ^2-pypz)}$_2$}], **4a**, showing the atom numbering. Ellipsoids are drawn at 30% probability.

Table 3 Selected distances (Å) and angles (°) for [Mn(μ^2-pypz)$_2${*fac*-{Mn(CO)$_3$(μ^2-pypz)}$_2$}], **4a**[17]

Mn(1)–C(1)	1.800(5)
Mn(1)–C(2)	1.800(4)
Mn(1)–C(3)	1.813(5)
Mn(1)–N(1)	2.087(3)
Mn(1)–N(2)	2.027(3)
Mn(1)–N(9)	2.051(3)
C(1)–O(1)	1.146(4)
C(2)–O(2)	1.147(4)
C(3)–O(3)	1.147(4)
Mn(3)–N(3)	2.257(3)
Mn(3)–N(8)	2.214(3)
Mn(3)–N(10)	2.331(3)
Mn(3)–N(11)	2.217(3)
C(1)–Mn(1)–C(2)	89.25(18)
C(1)–Mn(1)–C(3)	87.72(17)
C(2)–Mn(1)–C(3)	87.65(18)
C(1)–Mn(1)–N(1)	172.90(15)
C(2)–Mn(1)–N(1)	97.17(16)
C(3)–Mn(1)–N(1)	89.52(15)
C(1)–Mn(1)–N(2)	96.05(15)
C(2)–Mn(1)–N(2)	173.18(16)
C(3)–Mn(1)–N(2)	96.83(14)
C(1)–Mn(1)–N(9)	91.64(15)
C(2)–Mn(1)–N(9)	89.74(15)
C(3)–Mn(1)–N(9)	177.31(15)
N(2)–Mn(1)–N(9)	85.83(11)
N(1)–Mn(1)–N(2)	77.79(12)
N(1)–Mn(1)–N(9)	91.42(11)
N(8)–Mn(3)–N(11)	152.43(11)
N(8)–Mn(3)–N(3)	94.59(11)
N(11)–Mn(3)–N(3)	103.51(11)
N(8)–Mn(3)–N(6)	99.32(11)
N(11)–Mn(3)–N(6)	94.89(11)
N(3)–Mn(3)–N(6)	107.52(11)
N(8)–Mn(3)–N(10)	87.28(11)
N(11)–Mn(3)–N(10)	73.23(11)

Compound **4a** is a trimetallic molecule formed by a central "Mn^{II}(μ^2-pypz)^{2}" core, surrounded by two terminal "*fac*-{Mn^{I}(CO)$_3$(μ^2-pypz)}" moieties. The sixth coordination position of each terminal unit is occupied by a nitrogen atom of a bridging pyridylpyrazolate, which chelates the central manganese. Two chelated pyridylpyrazolates are coordinated to this central manganese, the other two positions being occupied by two nitrogen atoms, from each pyridylpyrazolate which chelates the terminal manganese atoms. Therefore, the structure allows to label the terminal manganese atoms as manganese(I), and the central metal atom as manganese(II).

The octahedral geometry of the terminal moieties is only slightly distorted, and their distances and angles are very similar. However, the octahedral geometry of the central manganese is severely distorted, as deduced from the *trans* N–Mn–N angles: N(3)–Mn(3)–N(7) 163.52(11)°, N(6)–Mn(3)–N(10) 163.16(11)°, and N(8)–Mn(3)–N(11) 152.43(11)°. The *cis* N–Mn–N angles are in the range 72.66(10)°–107.52(11)°. The dihedral angles of the pyridylpyrazolate chelating the central manganese (17° and 13°) are also larger than those found in those chelating the terminal units (6° and 7°).

A wide variety of *cis*-[Mn(N–N)$_2$X$_2$] (N–N: chelating N-donor ligand, X: halogen or pseudohalogen) have been described.[19] If the two nitrogen atoms coordinated to the central

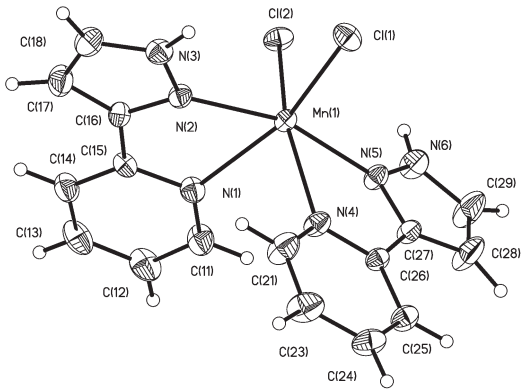

Fig. 7 Perspective view of *cis*-[$MnCl_2(pypzH)_2$], **5a**, showing the atom numbering. Ellipsoids are drawn at 30% probability.

Table 4 Selected distances (Å) and angles (°) for *cis*-[$MnCl_2(pypzH)_2$], **5a**

Mn(1)–N(1)	2.347(3)
Mn(1)–N(2)	2.245(3)
Mn(1)–N(4)	2.324(3)
Mn(1)–N(5)	2.231(3)
Mn(1)–Cl(1)	2.4634(12)
Mn(1)–Cl(2)	2.4640(12)
N(5)–Mn(1)–N(2)	163.16(12)
N(5)–Mn(1)–N(4)	70.57(12)
N(2)–Mn(1)–N(4)	98.44(12)
N(5)–Mn(1)–N(1)	95.78(12)
N(2)–Mn(1)–N(1)	70.33(11)
N(4)–Mn(1)–N(1)	86.91(12)
N(5)–Mn(1)–Cl(1)	104.09(9)
N(2)–Mn(1)–Cl(1)	89.12(8)
N(4)–Mn(1)–Cl(1)	94.34(9)
N(1)–Mn(1)–Cl(1)	159.34(8)
N(5)–Mn(1)–Cl(2)	87.27(9)
N(2)–Mn(1)–Cl(2)	101.33(9)
N(4)–Mn(1)–Cl(2)	156.67(9)
N(1)–Mn(1)–Cl(2)	88.21(9)
Cl(1)–Mn(1)–Cl(2)	98.19(4)

manganese, which belong to the pyridylpyrazolate chelated to the terminal moieties in **4a**, were substituted by two halides or pseudohalides, a similar complex *cis*-[$Mn(pypzH)_2X_2$] would be obtained. Therefore, we decided to synthesize this complex which, on the other hand, could be also an appropriate precursor to design a logical synthesis for the trimetallic complex **4a** (see below). Thus, the reaction of $MnCl_2{\cdot}4H_2O$ with two equivalents of pypzH in refluxing methanol led to *cis*-[$MnCl_2(pypzH)_2$], **5a**, as a white solid. The crystal structure of **5a** is depicted in Fig. 7, and Table 4 presents relevant distances and angles.

The geometry of **5a** shows distances and angles quite similar to those found in the central manganese of the trimetallic complex **4a**. Only the Cl–Mn–Cl angle (Cl(1)–Mn(1)–Cl(2) 98.22(4)°) in **5a** slightly differs from the corresponding N–Mn–N in **4a** (N(3)–Mn(3)–N(6) 107.52(11)°). The dihedral angles of the pyridylpyrazole in **5a** are also smaller (5° and 3°) than those found for the bridging pyridylpyrazolate in **4a** (17° and 13°). This is a well known feature also found when comparing chelating pyridylpyrazole and bridging pyridylpyrazolate.[8] The geometry of **5a** is also similar to those found for *cis*-[$Mn(N–N)_2X_2$] complexes.[19]

As indicated above, **5a** could be a precursor for the trimetallic species **4a**, if the chloride ligands were substituted by anionic "*fac*-{$Mn(CO)_3(\mu^2\text{-pypz})$}" fragments, after deprotonating also the pyridylpyrazole ligands. However, all the attempts made in this direction were unsuccessful.

Electrochemical behavior

The mononuclear Re^I *fac*-[$ReBr(CO)_3(pypzH)$] (**1b**), binuclear [*fac*-{$Re(CO)_3(\mu^2\text{-pypz})$}]$_2$ (**2b**) and heterometallic [{*fac*-$Re(CO)_3(\mu^2\text{-pypz})(\mu\text{-pypz})Na$}$_n$] (**3b**) complexes exhibit, by cyclic voltammetry (CV) (at 200 mV s^{-1}) at a platinum electrode and in 0.2 M [^{n}Bu$_4$N][BF_4]–THF, a first single-electron (for **1b**) or two-electron (CPE) (for **2b** and **3b**, *i.e.* one-electron/Re) irreversible (in the 0.05–4 V s^{-1} scan rate range tested) oxidation wave (wave $\mathbf{I^{ox}}$) at $^{I}E_p^{ox}$ = 1.61, 1.12 or 0.97 V *vs.* SCE, for **1b–3b**, respectively, assigned to the $Re^I \rightarrow Re^{II}$ oxidation process (in the cases of **2b** and **3b**, of the two Re^I centres) (Fig. 8, for **3b**).

A second irreversible oxidation process (wave $\mathbf{II^{ox}}$) is observed for **2b** and **3b** at a higher potential value ($^{II}E_p^{ox}$ = 1.49 or 1.30 V *vs.* SCE, for **2b** and **3b**, respectively), conceivably due to the $Re^{II} \rightarrow Re^{III}$ oxidation. The irreversibility of these oxidation waves ($\mathbf{I^{ox}}$ and $\mathbf{II^{ox}}$) indicates the instability of the resulting cationic Re complexes. Moreover, for all three Re^I complexes **1b–3b**, an irreversible cathodic process is observed (wave $\mathbf{I^{red}}$) at −1.74, −0.91 or −1.03 V *vs.* SCE, respectively.

The observation of a single oxidation wave, for the $Re^I \rightarrow Re^{II}$ process, in **2b** (instead of two distinct waves) is indicative of no significant electronic communication between the two Re^I metal centres, through the two bridging pyridylpyrazolates.

According to the literature data for other Re^I tricarbonyls with N-heterocyclic ligands, the first oxidation potential of **1b** ($^{I}E_p^{ox}$ = 1.61 V *vs.* SCE in THF) is only slightly higher than those reported, for the same anodic process ($Re^I \rightarrow Re^{II}$), for [$ReX(CO)_3L$] (X = halide; L = unsymmetrical bidentate iminopyridine ligand),[20] for the series *fac*-[$ReCl(CO)_3(pytri\text{-}R)$] [pytri-R =

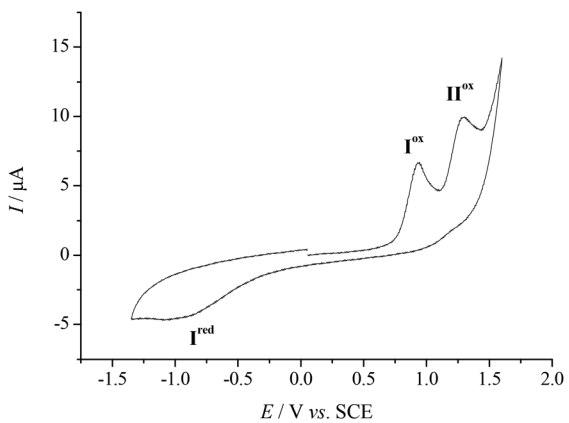

Fig. 8 Cyclic voltammogram of [{*fac*-$Re(CO)_3(\mu^2\text{-pypz})(\mu\text{-pypz})Na$}$_n$] (**3b**) (1.3 mM) (starting with the anodic scan), at a Pt electrode, in 0.2 M [^{n}Bu$_4$N][BF_4]–THF solution (v = 0.2 V s^{-1}).

2-(1-R-1*H*-1,2,3-triazol-4-yl)pyridine], or for *fac*-[ReCl(CO)$_3$-(py(CH$_2$)tri-R)][py(CH$_2$)tri-R = {(4-R-1*H*-1,2,3-triazol-1-yl)methyl}-pyridine].[21] It is significantly higher than those for *fac*-[ReX-(CO)$_3$L] (X = halide; L = diimine),[22] *fac*-[ReX(CO)$_3$(L^1/L^2)] (X = Cl or Br; L^1/L^2 = 1-alkyl-2-((*o*-thiomethyl)phenylazo)imidazole,[23] or *fac*-[ReBr(CO)$_3${H(pzAn^{Me})}] [H(pzAn^{Me}) = 2-(pyrazolyl)-4-toluidine].[24] The potential values reflect the electron-donor abilities of these *N*,*N*-ligands,[25] which thus can be ordered as follows: 1-alkyl-2-((*o*-thiomethyl)phenylazo)imidazole[23] > 2-(pyrazolyl)-4-toluidine[24] > diimine[22] > 2-(1-R-1*H*-1,2,3-triazol-4-yl)pyridine and {(4-R-1*H*-1,2,3-triazol-1-yl)methyl}pyridine[21] > (3-(2-pyridyl)pyrazole) [our work].

The lower oxidation potential of the binuclear complex [*fac*-{Re(CO)$_3$(μ^2-pypz)}]$_2$ (**2b**) or the bimetallic [{*fac*-Re(CO)$_3$-(μ^2-pypz)(μ-pypz)Na}$_n$] (**3b**) (1.12 or 0.97 V *vs.* SCE, in THF, for **2b** and **3b**, respectively) in comparison with that of the parent mononuclear *fac*-[ReBr(CO)$_3$(pypzH)] (**1b**) (1.61 V *vs.* SCE, in THF), reflects the stronger electron-donor character of the ligands in **2b** or **3b** (two μ^2-pypz), for each metal center, relative to those in **1b** (Br$^-$ + pypzH). In terms of the electrochemical Lever E_L parameter[24] (the lower this value, the stronger is the ligand electron-donor character) one can conclude that the sums of E_L values for the two μ^2-pypz ligands (in **2b** and **3b**) are lower than those of Br$^-$ + bidentate pypzH (in **1b**).

The monomeric manganese(I) *fac*-[MnBr(CO)$_3$(pypzH)] **1a** exhibits two irreversible oxidation waves (**I^{ox}** and **II^{ox}**) at 1.22 and 1.52 V *vs.* SCE (at 200 mV s^{-1}) assigned to the Mn^I → Mn^{II} and Mn^{II} → Mn^{III} oxidations, similarly to the case of the analogous Re^I complex **1b**.

Complex **1a** also shows a reduction wave at E_p^{red} = −1.56 V *vs.* SCE (**I^{red}**, Fig. 9). Moreover, upon scan reversal after the reduction wave, a new irreversible oxidation process is detected at E_p^{ox} of *ca.* 0.8 V *vs.* SCE (Fig. 9). This new wave conceivably concerns the oxidation of the bromide ion liberated upon reduction. The involvement of the bromide ion is supported by the independently measured values ($^IE_p^{ox}$ = 0.9 and $^{II}E_p^{ox}$ = 1.3 V *vs.* SCE) of the irreversible oxidation waves of tetrabutylammonium bromide under the same experimental conditions (the second wave is buried under the oxidation wave of the complex). Moreover, this is confirmed by the increase of the current intensity of this new wave and of the oxidation wave of **1a** (which overlaps with the second oxidation wave of Br$^-$), upon addition of [^{n}Bu$_4$N]Br to the CV solution.

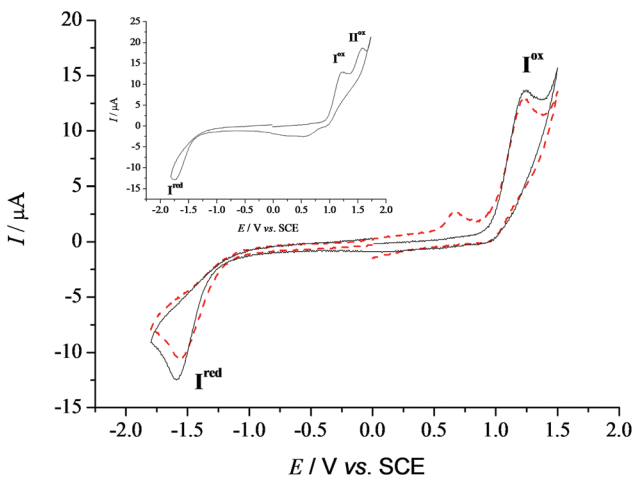

Fig. 9 Cyclic voltammograms of *fac*-[Mn(CO)$_3$Br(pypzH)] (**1a**) (6.2 mM) (anodic scan), at a Pt electrode, in 0.2 M [^{n}Bu$_4$N][BF$_4$]–THF solution (*v* = 200 mV s^{-1}). Full line: initiated with the anodic scan. Dotted line: initiated with the cathodic scan. Inset: extended anodic sweep beyond the second oxidation wave.

Table 5 Cyclic voltammetric data[a] for *fac*-[MnBr(CO)$_3$(pypzH)] (**1a**), [{*fac*-Mn(CO)$_3$(μ^2-pypz)(μ^3-pypz)M′}$_n$] [M′ = Li, Li-**3a**, *n* = 1; Na, Na-**3a**, *n* = 2, and K, K-**3a**, *n* = 2], [{*fac*-Mn(μ^2-pypz)$_2$(*fac*-{Mn(CO)$_3$(μ^2-pypz)}$_2$}] (**4a**), *cis*-[MnCl$_2$(pypzH)$_2$] (**5a**), *fac*-[ReBr(CO)$_3$(pypzH)] (**1b**), [*fac*-{Re-(CO)$_3$(μ^2-pypz)}]$_2$ (**2b**) [{*fac*-Re(CO)$_3$(μ^2-pypz)(μ-pypz)Na}$_n$] (**3b**)

Complex	$^IE_p^{ox}$ ($^IE_{1/2}^{ox}$)	$^{II}E_p^{ox}$	$^IE_p^{red}$
1b	1.62	—	−1.06
2b	1.12	1.49	−0.91
3b	0.97	1.30	−1.03
1a	1.22	1.52	−1.56
Li-**3a**	0.80	1.40	—
Na-**3a**	0.62	1.02	—
K-**3a**	0.62	1.05	—
4a	(0.90)	1.36	—
5a	(0.96)	—	—

[a] Values in V ± 0.02 relative to SCE (see the Experimental section); scan rate of 200 mV s^{-1}. Values for reversible waves are given in parentheses.

The complexes [{*fac*-Mn(CO)$_3$(μ^2-pypz)(μ^3-pypz)M′}$_n$] [M′ = Li, Li-**3a**, *n* = 1; Na, Na-**3a**, *n* = 2, and K, K-**3a**, *n* = 2] exhibit, by CV, two single-electron irreversible oxidation waves, the first one (wave **I^{ox}**) at potential values in the range of 0.62–0.8 V *vs.* SCE (Table 5), followed by the second one (wave **II^{ox}**) at higher potential values (1.02–1.4 V *vs.* SCE) (Table 5). Moreover, for complexes Na-**3a** and K-**3a** a third irreversible oxidation wave is observed at $^{III}E_p^{ox}$ = 1.47 and 1.39 V *vs.* SCE, respectively. No clear reduction waves were detected for these Mn complexes.

The above manganese(I) complexes **1a** and Na-**3a** are oxidized at lower potentials (by *ca.* 0.35–0.4 V) than the analogous rhenium(I) complexes (**1b** and **3b**, respectively). This is in accordance with the relative behavior reported for other rhenium(I) and manganese(I) complexes, namely *fac*-[MBr-(CO)$_3${H(pzAn^{Me})}] [M = Mn, Re; H(pzAn^{Me}) = 2-(pyrazolyl)-4-toluidine].[24]

The paramagnetic mixed-valence Mn^I/Mn^{II} complex **4a** exhibits by CV a first reversible two-electron oxidation (wave **I^{ox}**) at $^IE_{1/2}^{ox}$ = 0.90 V *vs.* SCE, attributed to the Mn^I → Mn^{II} oxidation processes of both Mn^I metal centres, followed, at a higher potential value, by a second irreversible oxidation (wave **II^{ox}**) at $^{II}E_p^{ox}$ = 1.36 V *vs.* SCE, conceivable due to Mn^{II} → Mn^{III} oxidation. The paramagnetic mononuclear Mn^{II} dichlorocomplex **5a** shows a single-electron reversible oxidation process (wave **I^{ox}**) at $^IE_{1/2}^{ox}$ = 0.96 V *vs.* SCE.

Although compound **4a** has been synthesised starting from compound **3a**, controlled potential electrolysis at the first oxidation wave of the latter has not led to the former.

Conclusions

The deprotonation of pyridylpyrazole coordinated to bromidotricarbonylrhenium is straightforward and gives the corresponding bimetallic complex with a bridging pyridylpyrazolate. However, the same process with the manganese complex affords heteropolymetallic complexes where pyridylpyrazolate bridges manganese and the alkali metal atom. Those with sodium and potassium are tetrametallic complexes containing two manganese and two alkali metal atoms and a bridging pyridylpyrazolate ligand with an unprecedented coordination mode: the nitrogen of the pyridyl fragment and the nitrogen-1 of pyrazolate are chelated to manganese atoms, whereas each nitrogen-2 of pyrazolate is coordinated to two alkali metal atoms. On the other hand, the lithium complex is heterobimetallic and contains a very uncommon chelating pyridylpyrazolate. Hence, the size of the alkali metal atoms determines the final structure of the heterometallic complexes: lithium is tetracoordinated whereas sodium and potassium are pentacoordinated; the larger the metal, the bulkier the ligands surrounding them. The coordination of transition metals instead of these alkali metals is currently under investigation. The heteropolymetallic complexes evolve spontaneously to the parent homobimetallic pyridylpyrazolate bridging complex in the case of rhenium, and to a trimanganese paramagnetic complex ($Mn^{I}Mn^{II}Mn^{I}$).

Experimental

General procedures

All manipulations were performed under a N_2 atmosphere following conventional Schlenk techniques. Filtrations were carried out on dry Celite without exclusion of air. Solvents were purified according to standard procedures.[26] *fac*-[$MnBr(CO)_3(NCMe)_2$],[7a] *fac*-[$ReBr(CO)_3(NCMe)_2$],[27] and 3-(2-pyridyl)pyrazole[28] were obtained as previously described. All other reagents were obtained from the usual commercial suppliers, and used as received. Infrared spectra were recorded in a Perkin-Elmer RX I FT-IR apparatus using 0.2 mm CaF_2 cells for solutions or on KBr pellets for solid samples. NMR spectra were recorded in Bruker AC-300, ARX-300, or AV-400 in Me_2CO-d_6 at room temperature (r.t.) unless otherwise stated. NMR spectra are referred to the internal residual solvent peak for ^1H and $^{13}C\{^1H\}$ NMR. Assignment of the ^1H NMR spectra was supported by COSY experiments and assignment of $^{13}C\{^1H\}$ NMR data was supported by DEPT experiments and relative intensities of the resonance signals or HSQAD experiments. Elemental analyses were performed on a Perkin-Elmer 2400B microanalyzer (Fig. 10).

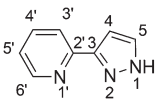

Fig. 10 Numbering of pypzH for NMR assignment.

***fac*-[MnBr(CO)$_3$(pypzH)], 1a.** To a recently prepared solution of *fac*-[$MnBr(CO)_3(NCMe)_2$] (obtained from 0.274 g of [$MnBr(CO)_5$], 1 mmol) in CH_2Cl_2 (30 mL), 3-(2-pyridyl)pyrazole (0.145 g, 1 mmol) was added. The solution was stirred at r.t. for 1 h. The yellow solid which precipitated during this time was decanted, washed with hexane (3 × 5 mL) and dried *in vacuo*, yielding 0.322 g (88%). IR (THF, cm^{-1}): 2024 vs, 1935 vs, 1913 vs. IR (KBr, cm^{-1}): 3145 w, 2028 vs, 1933 vs, 1910 vs, 1615 w, 1458 w, 1376 w, 1090 w, 767 m, 685 w, 630 w. ^1H NMR: 7.24 (br s, H^4 pzH, 1 H), 7.58 (m, H^5 py, 1 H), 8.16 (m, H^3 py, H^4 py, and H^5 pzH, 3 H), 9.17 (d, J = 4.5 Hz, H^6 py, 1 H), 13.75 (br s, N*H* pzH, 1 H). $^{13}C\{^1H\}$ NMR: 105.0 (s, C^4 pzH), 122.6 (s, C^3 py), 125.5 (s, C^5 py), 135.4 (s, C^5 pzH), 139.7 (s, C^4 py), 152.4 (s, C^3 pzH or C^2 py), 152.6 (s, C^3 pzH or C^2 py), 154.4 (s, C^6 py), 212.6 (s, *C*O), 223.3 (s, *C*O), 223.7 (s, *C*O). Anal. calcd for $C_{11}H_7BrMnN_3O_3$: C, 36.29; H, 1.94; N, 11.54. Found: C, 36.58; H, 1.97; N, 11.54.

***fac*-[ReBr(CO)$_3$(pypzH)], 1b.** 3-(2-Pyridyl)pyrazole (0.029 g, 0.2 mmol) was added to a solution of *fac*-[$ReBr(CO)_3(NCMe)_2$] (0.086 g, 0.2 mmol) in CH_2Cl_2 (10 mL). The solution was stirred at r.t. for 1 h. The pale yellow which precipitated during this time was decanted, washed with hexane (3 × 3 mL) and dried *in vacuo*, yielding 0.081 g (82%). IR (THF, cm^{-1}): 2024 vs, 1935 vs, 1893 vs. IR (KBr, cm^{--1}): 3146 w, 2022 vs, 1920 vs, 1879 vs, 1613 w, 1432 w, 1373 w, 112 w, 1091 m, 767 m, 644 w. ^1H NMR: 7.30 (dd, J = 3, and 2 Hz, H^4 pzH, 1 H), 7.62 (ddd, J = 7.5, 5.5, and 1 Hz, H^5 py, 1 H), 8.17 (dd, J = 3, and 1 Hz, H^5 pzH, 1 H), 8.21 (ddd, J = 9.5, 7.5, and 1.5 Hz, H^4 py, 1 H), 8.29 (dd, J = 9.5, and 1 Hz, H^3 py, 1 H), 9.03 (dd, J = 5.5, and 1.5 Hz, H^6 py, 1 H), 13.97 (br s, N*H* pzH, 1 H). $^{13}C\{^1H\}$ NMR: 105.7 (s, C^4 pzH), 123.4 (s, C^3 py), 126.6 (s, C^5 py), 134.7 (s, C^5 pzH), 140.7 (s, C^4 py), 152.2 (s, C^3 pzH or C^2 py), 153.8 (s, C^3 pzH or C^2 py), 153.9 (s, C^6 py), 189.4 (s, *C*O), 196.7 (s, *C*O), 198.1 (s, *C*O). Anal. calcd for $C_{11}H_7BrN_3O_3Re$: C, 26.67; H, 1.42; N, 8.48. Found: C, 26.93; H, 1.46; N, 8.41.

[*fac*-{Re(CO)$_3$(μ^2-pypz)}]$_2$, 2b. A 1 M solution of NaOMe in MeOH (0.3 mmol) was added dropwise to a solution of **1b** (0.148 g, 0.3 mmol) in THF (10 mL) and the mixture was stirred at r.t. for 15 min. Then the solution was filtered and concentrated *in vacuo*. Addition of hexane (*ca*. 10 mL) and cooling to −20 °C yielded yellow crystals which were decanted, washed with hexane (3 × 3 mL), and dried *in vacuo*, yielding 0.042 g (34%). IR (THF, cm^{-1}): 2030 vs, 1917 vs, 1894 vs. IR (KBr, cm^{-1}): 2026 vs, 2010 vs, 1884 vs, 1611 m, 1456 w, 1359 w, 1098 w, 763 m. ^1H NMR: 6.57 (d, J = 2.5 Hz, H^4 pz, 1 H), 7.49 (td, J = 5.5, and 1 Hz, H^5 py, 1 H), 7.69 (d, J = 2 Hz, H^4 py, 1 H), 7.86 (d, J = 7.5 Hz, H^5 pz, 1 H), 8.05 (dt, J = 8, and 2 Hz, H^3 py, 1 H), 9.18 (d, J = 5.5 Hz, H^6 py, 1 H). $^{13}C\{^1H\}$ NMR: 106.0 (s, C^4 pz), 121.5 (s, C^3 py), 124.9 (s, C^5 py), 140.7 (s, C^5 pz), 144.5 (s, C^4 py), 153.1 (s, C^6 py), 154.6 (s, C^3 pz or C^2 py), 154.8 (s, C^3 pz or C^2 py), 198.1 (s, *C*O), 197.0 (s, *C*O), 198.3 (s, *C*O). Anal. calcd for $C_{22}H_{12}N_6O_6Re_2$: C, 31.88; H, 1.46; N, 10.14. Found: C, 31.60; H, 1.27; N, 10.39.

[*fac*-Mn(CO)$_3$(μ^2-pypz)(μ^2-pypz)Li(OH$_2$)(THF)], Li-3a. A LiOMe 1 M solution in MeOH (1 mL, 1 mmol) was added to a solution of **1a** (0.182 g, 0.5 mmol) and pypzH (0.073 g,

0.5 mmol) in THF (20 mL). The mixture was stirred at r.t. for 15 min. Then the solution was filtered and concentrated *in vacuo*. Addition of hexane (*ca*. 10 mL) and cooling to −20 °C yielded yellow crystals which were decanted, washed with hexane (3 × 3 mL), and dried *in vacuo*, yielding 0.183 g (70%). IR (THF, cm^{-1}): 2019 vs, 1922 vs, 1905 vs. IR (cm^{-1}): 2014 vs, 1913 vs, 1891 vs, 1596 m, 1450 m, 1429 m, 1354 w, 1050 m, 756 s, 633 w. ^{1}H NMR: 6.36 (s, H^4 pzMn, 1 H), 6.62 (s, H^4 pzLi, 1 H), 6.85 (s, H^5 pzMn, 1 H), 7.10 (t, J = 3 Hz, H^5 pyMn, 1 H), 7.32 (t, J = 5 Hz, H^5 pyLi, 1 H), 7.48 (d, J = 8 Hz, H^3 pyMn, 1 H), 7.55 (s, H^5 pzLi, 1 H), 7.64 (d, J = 8 Hz, H^3 pyLi, 1 H), 7.72 (t, J = 8 Hz, H^4 pyMn, 1 H), 7.88 (t, J = 8 Hz, H^4 pyLi, 1 H), 8.34 (d, J = 3 Hz, H^6 pyMn, 1 H), 9.13 (d, J = 5 Hz, H^6 pyLi, 1 H). ^{13}C{^{1}H} NMR: 101.8 (s, C^4 pzMn), 102.0 (s, C^4 pzLi), 118.7 (s, C^3 pyMn), 119.0 (s, C^3 pyLi), 120.7 (s, C^5 pyMn), 121.5 (s, C^5 pyLi), 137.7 (s, C^4 pyMn), 138.2 (s, C^4 pyLi), 140.0 (s, C^5 pzMn), 141.4 (s, C^5 pzLi), 148.3 (s, C^6 pyMn), 152.4 (s, C^6 pyLi), 220.1 (s, *C*O), 221.2 (s, *C*O), 223.0 (s, *C*O). Anal. calcd for $C_{23}H_{22}LiMnN_6O_5$: C, 52.68; H, 4.23; N, 16.03. Found: C, 51.46; H, 4.45; N, 15.65.

[{*fac*-Mn(CO)$_3$(μ^2-pypz)(μ^3-pypz)Na}$_2$], Na-3a. A solution of Napypz previously prepared from the addition of a 1 M NaOMe solution in MeOH (0.6 mL, 0.6 mmol) to 3-(2-pyridyl)pyrazole (0.087 g, 0.6 mmol) in THF (10 mL) was added to a recently prepared solution of *fac*-[MnBr(CO)$_3$(NCMe)$_2$] (obtained from 0.083 g of [MnBr(CO)$_5$], 0.3 mmol), in THF (10 mL). The mixture was stirred at r.t. for 5 min. Then the solution was filtered and concentrated *in vacuo*. Addition of hexane (*ca*. 10 mL) and cooling to −20 °C yielded orange crystals which were decanted, washed with hexane (3 × 3 mL), and dried *in vacuo*, yielding 0.114 g (73%). IR (THF, cm^{-1}): 2016 vs, 1919 vs, 1900 vs. IR (KBr, cm^{-1}): 2017 vs, 1932 vs, 1880 vs, 1871 vs, 1610 w, 1592 w, 1353 w, 1120 w, 760 m, 636 w. ^{1}H NMR: 6.37 (d, J = 2 Hz, H^4 pzMn, 1 H), 6.59 (d, J = 2.5 Hz, H^4 pzNa, 1 H), 7.00 (td, J = 5.5, and 1 Hz, H^5 pyMn, 1 H), 7.21 (d, J = 2 Hz, H^5 pzMn, 1 H), 7.31 (td, J = 5.5 Hz, and 1 Hz, H^5 pyNa, 1 H), 7.45 (d, J = 8 Hz, H^3 pyMn, 1 H), 7.52 (d, J = 2 Hz, H^5 pzNa, 1 H), 7.62 (m, H^4 pyMn, and H^3 pyNa, 2 H), 7.85 (td, J = 8, and 2 Hz, H^4 pyNa, 1 H), 8.28 (d, J = 4.5 Hz, H^6 pyMn, 1 H), 9.15 (d, J = 5.5 Hz, H^6 pyNa, 1 H). ^{13}C{^{1}H} NMR: 101.7 (s, C^4 pzMn), 102.0 (s, C^4 pzNa), 118.8 (s, C^3 pyMn), 119.0 (s, C^3 pyNa), 120.1 (s, C^5 pyMn), 121.3 (s, C^5 pyNa), 136.8 (s, C^4 pyMn), 138.0 (s, C^4 pyNa), 140.1 (s, C^5 pzMn), 142.2 (s, C^5 pzNa), 148.76 (s, C^6 pyMn), 152.2 (s, C^6 pyNa), *C*O not observed. Anal. calcd for $C_{38}H_{24}Mn_2N_{12}Na_2O_6$: C, 50.68; H, 2.69; N, 18.66. Found: C, 50.69; H, 2.35; N, 18.75.

[{*fac*-Mn(CO)$_3$(μ^2-pypz)(μ^3-pypz)K(THF)}$_2$], K-3a. A 1 M KOMe solution in MeOH (1 mL, 1 mmol) was added to a solution of **1a** (0.182 g, 0.5 mmol) and pypzH (0.073 g, 0.5 mmol) in THF (20 mL). The mixture was stirred at r.t. for 15 min. Then the solution was filtered and concentrated *in vacuo*. Addition of hexane (*ca*. 10 mL) and cooling to −20 °C yielded yellow crystals which were decanted, washed with hexane (3 × 3 mL), and dried *in vacuo*, yielding 0.192 g (76%). IR (THF, cm^{-1}): 2015 vs, 1910 vs, 1904 vs. IR (cm^{-1}): 2009 vs, 1889 vs br, 1596 m, 1450 m, 1426 m, 1350 w, 1054 m, 754 s, 634 m, 536 w, 393 w. ^{1}H NMR: 6.34 (s, H^4 pzMn, 1 H), 6.59 (s, H^4 pzK, 1 H), 6.91 (s, H^5 pzMn, 1 H), 6.96 (t, J = 2 Hz, H^5 pyMn, 1 H), 7.27 (t, J = 2 Hz, H^5 pyLi, 1 H), 7.51 (s, H^5 pzK, 1 H), 7.55 (m, H^3 pyMn, H^3 pyK, and H^4 pyMn, 3 H), 7.83 (t, J = 2 Hz, H^4 pyK, 1 H), 8.35 (d, J = 2 Hz, H^6 pyMn, 1 H), 9.13 (d, J = 5 Hz, H^6 pyK, 1 H). ^{13}C{^{1}H} NMR: 101.6 (s, C^4 pzMn), 102.1 (s, C^4 pzK), 118.6 (s, C^3 pyMn), 119.1 (s, C^3 pyK), 119.6 (s, C^5 pyMn), 120.9 (s, C^5 pyK), 136.1 (s, C^4 pyMn), 137.8 (s, C^4 pyK), 139.1 (s, C^5 pzMn), 141.0 (s, C^5 pzK), 148.6 (s, C^6 pyMn), 152.3 (s, C^6 pyK), *C*O not observed. Anal. calcd for $C_{47}H_{44}K_2Mn_2N_{12}O_9$ (K-3a·MeOH): C, 50.90; H, 4.00; N, 12.98. Found: C, 50.74; H, 4.01; N, 13.18.

[{*fac*-Re(CO)$_3$(μ^2-pypz)(μ-pypz)Na}$_n$], 3b. A solution of Napypz previously prepared from the addition of a 1 M NaOMe solution in MeOH (0.6 mL, 0.6 mmol) to 3-(2-pyridyl)pyrazole (0.087 g, 0.6 mmol) in THF (10 mL) was added to a solution of *fac*-[Re(CO)$_3$Br(NCMe)$_2$] (0.149 g, 0.3 mmol) in THF (10 mL). The solution was stirred at r.t. for 10 min. Then the solution was filtered and concentrated *in vacuo*. Addition of hexane (*ca*. 10 mL) and cooling to −20 °C yielded orange crystals which were decanted, washed with hexane (3 × 3 mL), and dried *in vacuo*, yielding 0.127 g (65%). IR (THF, cm^{-1}): 2008 vs, 1883 vs br. IR (cm^{-1}): 2003 vs, 1857 vs br, 1612 m, 1595 m, 1566 w, 1537 w, 1515 w, 1454 m, 1428 m, 1352 m, 1130 w, 1096 w, 1053 m, 882 w, 759 s, 709 w, 627 w. ^{1}H NMR: 6.36 (s, H^4 pzRe, 1 H), 6.61 (s, H^4 pzNa, 1 H), 7.06 (t, J = 5 Hz, H^5 pyRe, 1 H), 7.27 (s, H^5 pzRe, 1 H), 7.34 (t, J = 5 Hz, H^5 pyNa, 1 H), 7.48 (s, H^5 pzNa, 1 H), 7.49 (d, J = 2 Hz, H^3 pyRe, 1 H), 7.66 (t, J = 7 Hz, H^4 pyRe, 1 H), 7.72 (d, J = 10 Hz, H^3 pyNa, 1 H), 7.95 (t, J = 7 Hz, H^4 pyNa, 1 H), 8.30 (d, J = 5 Hz, H^6 pyRe, 1 H), 9.08 (d, J = 5 Hz, H^6 pyNa, 1 H). ^{13}C{^{1}H} NMR: 101.8 (s, C^4 pzRe), 102.7 (s, C^4 pzNa), 119.3 (s, C^3 pyRe), 119.7 (s, C^3 pyNa), 122.3 (s, C^5 pyRe), 124.0 (s, C^5 pyNa), 136.9 (s, C^4 pyRe), 139.0 (s, C^4 pyNa), 140.0 (s, C^5 pzRe), 141.7 (s, C^5 pzNa), 148.9 (s, C^6 pyRe), 151.9 (s, C^6 pyNa), 195.9 (s, *C*O), 198.7 (s, *C*O), 199.8 (s, *C*O). Anal. calcd for $C_{38}H_{24}N_{12}Na_2O_6Re_2$: C, 39.24; H, 2.08; N, 14.45. Found: C, 39.29; H, 2.47; N, 14.19.

[Mn(μ^2-pypz)$_2${*fac*-{Mn(CO)$_3$(μ^2-pypz)}$_2$}], 4a. Precipitated as yellow needles from solutions of **3a** after several days. IR (THF, cm^{-1}): 2026 vs, 1935 vs, 1907 vs. IR (KBr, cm^{-1}): 2023 vs, 1929 vs, 1901 vs, 1773 w, 1599 m, 1451 m, 1429 w, 1354 w, 1153 w, 1116 w, 1093 w, 1064 w, 758 m. Anal. calcd for $C_{38}H_{24}Mn_3N_{12}O_6$: C, 50.18; H, 2.66; N, 18.48. Found: C, 50.02; H, 2.44; N, 18.71.

***cis*-[MnCl$_2$(pypzH)$_2$], 5a.** 3-(2-Pyridyl)pyrazole (0.145 g, 1 mmol) was added to a solution of $MnCl_2·4H_2O$ (0.063 g, 0.5 mmol) in MeOH (10 mL) and the solution was refluxed for 2 h. Then the solution was concentrated *in vacuo*, and cooled to −20 °C. The colorless crystals obtained were decanted, washed with hexane (3 × 3 mL), and dried *in vacuo*, yielding 0.165 g (80%). IR (KBr, cm^{-1}): 3200 s, 2958 m, 1603 s, 1457 s, 1431 s, 1363 m, 1093 m, 969 m, 780 s, 634 w. Anal. calcd for $C_{16}H_{14}Cl_2MnN_6$: C, 46.18; H, 3.39; N, 20.19. Found: C, 45.89; H, 3.37; N, 19.95.

Crystal structure determination for compounds 2b, Li-3a, Na-3a, K-3a, 4a, and 5a

Crystals were grown in MeOH (for **5a**) or by slow diffusion of hexane into concentrated solutions of the complexes in THF (for **2b**, **3a**, and **4a**) at −20 °C. Relevant crystallographic details are given in Table 5. A crystal was attached to a glass fiber and transferred to a Bruker AXS SMART 1000 diffractometer with graphite monochromatized Mo K_α X-radiation and a CCD area detector. Raw frame data were integrated with the SAINT program.[29] The structure was solved by direct methods with SHELXTL.[30] A semi-empirical absorption correction was applied with the program SADABS.[31] All non-hydrogen atoms were refined anisotropically. Hydrogen atoms were set in calculated positions and refined as riding atoms, with a common thermal parameter. All calculations and graphics were made with SHELXTL. Distances and angles of hydrogen bonds were calculated with PARST[32] (normalized values).[33] CCDC 873520 (**2b**), 974910 (Li-**3a**), 873521 (Na-**3a**), 974911 (K-**3a**), 873522 (**4a**), and 873523 (**5a**) contain the detailed crystallographic data for this publication.

Electrochemical studies

The electrochemical experiments were performed on an EG&G PAR 273A potentiostat/galvanostat connected to a personal computer through a GPIB interface. Cyclic voltammetry (CV) studies were undertaken in 0.2 M $[^nBu_4N][BF_4]$–THF, at a platinum disc working electrode (d = 0.5 mm) and at room temperature. Controlled-potential electrolyses (CPE) were carried out in electrolyte solutions with the above-mentioned composition, in a three-electrode H-type cell. The compartments were separated by a sintered glass frit and equipped with platinum gauze working and counter-electrodes. For both CV and CPE experiments, a Luggin capillary connected to a silver wire pseudo-reference electrode was used to control the working electrode potential. A Pt wire was employed as the counter-electrode for the CV cell. The CPE experiments were monitored regularly by cyclic voltammetry, thus ensuring that no significant potential drift occurred along the electrolyses. The solutions were saturated with N_2 by bubbling this gas before each run, and the redox potentials of the complexes were measured by CV in the presence of ferrocene as the internal standard, and their values are quoted relative to the SCE by using the $[Fe(\eta^5\text{-}C_5H_5)_2]^{0/+}$ redox couple (E = 0.545 V *vs.* SCE).[34]

Acknowledgements

The authors thank the Spanish Ministerio de Ciencia e Innovación (CTQ2009-12111) and the Junta de Castilla y León (VA070A08 and GR Excelencia 125) for financial support. M. A. and R. G.-R. thank the MEC (FPI and FPU Programs respectively) and P. G.-I. the UVa for their grants. The work was also partially supported by the Foundation for Science and Technology (FCT, Portugal, project Pest-OE/QUI/UI0100/2013).

Notes and references

1 See for example: (*a*) L.-A. Chen, W. Xu, B. Huang, J. Ma, L. Wang, J. Xi, K. Harms, L. Gong and E. Meggers, *J. Am. Chem. Soc.*, 2013, **135**, 10598–10601; (*b*) R. M. Edkins, D. Sykes, A. Beeby and M. D. Ward, *Chem. Commun.*, 2012, **48**, 9977–9979; (*c*) A. C. Coelho, M. Nolasco, S. S. Balula, M. M. Antunes, C. C. L. Pereira, F. A. A. Paz, A. A. Valente, M. Pillinger, P. Ribeiro-Claro, J. Klinowski and I. S. Gonçalves, *Inorg. Chem.*, 2011, **50**, 525–538; (*d*) M. Dakkach, M. I. López, I. Romero, M. Rodríguez, A. Atlamsani, T. Parella, X. Fontrodona and A. Llobet, *Inorg. Chem.*, 2010, **49**, 7072–7079; (*e*) V. Montoya, J. Pons, V. Branchadell, J. García-Antón, X. Solans, M. Font-Bardia and J. Ros, *Organometallics*, 2008, **27**, 1084–1091; (*f*) J. S. Uber, Y. Vogels, D. van den Helder, I. Mutikainen, U. Turpeinen, W. T. Fu, O. Roubeau, P. Gamez and J. Reedijk, *Eur. J. Inorg. Chem.*, 2007, 4197–4206; (*g*) J. Mukherjee and R. Mukherjee, *Dalton Trans.*, 2006, 1611–1621; (*h*) A. Satake and T. Nakata, *J. Am. Chem. Soc.*, 1998, **120**, 10391–10396.

2 (*a*) D. Sykes, S. C. Parker, I. V. Sazanovich, A. Stephenson, J. A. Weinstein and M. D. Ward, *Inorg. Chem.*, 2013, **52**, 10500–10511; (*b*) P. Ovejero, E. Asensio, J. V. Heras, J. A. Campo, M. Cano, M. R. Torres, C. Núñez and C. Lodeiro, *Dalton Trans.*, 2013, **42**, 2107–2120; (*c*) Y. Chi and P.-T. Chou, *Chem. Soc. Rev.*, 2007, **36**, 1421–1431; (*d*) P.-T. Chou and Y. Chi, *Eur. J. Inorg. Chem.*, 2006, 3319–3332.

3 (*a*) B. A. Leita, B. Moubaraki, K. S. Murray, J. P. Smith and J. D. Cashion, *Chem. Commun.*, 2004, 156–157; (*b*) A. J. Metherell, W. Cullen, A. Stephenson, C. A. Hunter and M. D. Ward, *Dalton Trans.*, 2014, **43**, 71–84.

4 P. L. Jones, J. C. Jeffery, J. A. McCleverty and M. D. Ward, *Polyhedron*, 1997, **16**, 1567–1571.

5 Some examples of homopolymetallic complexes: (*a*) J. C. Jeffery, P. L. Jones, K. L. V. Mann, E. Psillakis, J. A. McCleverty, M. D. Ward and C. M. White, *Chem. Commun.*, 1997, 175–176; (*b*) K. Singh, J. R. Long and P. Stavropoulos, *Inorg. Chem.*, 1998, **37**, 1073–1079; (*c*) K. L. V. Mann, E. Psillakis, J. C. Jeffery, L. H. Rees, N. M. Harden, J. A. McCleverty, M. D. Ward, D. Gatteschi, F. Totti, F. E. Mabbs, E. J. L. McInnes, P. C. Riedi and G. M. Smith, *J. Chem. Soc., Dalton Trans.*, 1999, 339–348; (*d*) S. Zein and S. A. Borshch, *J. Am. Chem. Soc.*, 2005, **127**, 16197–16201; (*e*) T.-L. Hu, J.-R. Li, C.-S. Liu, X.-S. Shi, J.-N. Zhou, X.-H. Bu and J. Ribas, *Inorg. Chem.*, 2006, **45**, 162–173; (*f*) S.-Y. Chang, J.-L. Chen, Y. Chi, Y.-M. Cheng, G.-H. Lee, C.-M. Jiang and P.-T. Chou, *Inorg. Chem.*, 2007, **46**, 11202–11212; (*g*) Q. F. Mokuolu, D. Foguet-Albiol, L. F. Jones, J. Wolowska, R. M. Kowalczyk, C. A. Kilner, C. Christou, P. C. McGowan and M. A. Halcrow, *Dalton Trans.*, 2007, 1392–1399; (*h*) V. Mishra, F. Lloret and R. Mukherjee, *Eur. J. Inorg. Chem.*, 2007, 2161–2170; (*i*) T.-L. Hu, R.-Q. Zou, J.-R. L and X.-H. Bu, *Dalton Trans.*, 2008, 1302–1311; (*j*) J. Mola, C. Dinoi, X. Sala,

M. Rodríguez, I. Romero, T. Parella, X. Fontrodona and A. Llobet, *Dalton Trans.*, 2011, **40**, 3640–3646.

6 (*a*) M.-L. Ho, Y.-M. Cheng, L.-C. Wu, P.-T. Chou, G.-H. Lee, F.-C. Hsu and Y. Chi, *Polyhedron*, 2007, **26**, 4886–4892; (*b*) M. H. W. Lam, S. T. C. Cheung, K.-M. Fung and W.-T. Wong, *Inorg. Chem.*, 1997, **36**, 4618–4619.

7 (*a*) M. Arroyo, A. López-Sanvicente, D. Miguel and F. Villafañe, *Eur. J. Inorg. Chem.*, 2005, 4430–4437; (*b*) M. Arroyo, D. Miguel, F. Villafañe, S. Nieto, J. Pérez and L. Riera, *Inorg. Chem.*, 2006, **45**, 7018–7026; (*c*) N. Antón, M. Arroyo, P. Gómez-Iglesias, D. Miguel and F. Villafañe, *J. Organomet. Chem.*, 2008, **693**, 3074–3080; (*d*) M. Arroyo, P. Gómez-Iglesias, J. M. Martín-Alvarez, C. M. Alvarez, D. Miguel and F. Villafañe, *Inorg. Chem.*, 2012, **51**, 6070–6080.

8 M. Arroyo, D. Miguel, F. Villafañe, E. C. B. Alegria and A. J. L. Pombeiro, *Dalton Trans.*, 2012, **41**, 7017–7025.

9 S. Mukherjee, Y. P. Patil and P. S. Mukherjee, *Inorg. Chem.*, 2012, **51**, 4888–4890, and references therein.

10 (*a*) T. S. Venkatakrishnan, M. Nethaji and S. S. Krishnamurthy, *J. Organomet. Chem.*, 2006, **691**, 224–228; (*b*) C. C. Quitmann, R. Bezugly, F. Wagner and K. Müller-Buschbaum, *Z. Anorg. Allg. Chem.*, 2006, **632**, 1173–1186; (*c*) T. Beringhelli, G. D'Alfonso, M. Panigati, P. Mercandelli and A. Sironi, *Chem.–Eur. J.*, 2002, **8**, 5340–5350; (*d*) G. B. Deacon, E. E. Delbridge, C. M. Forsyth, B. W. Skelton and A. H. White, *J. Chem. Soc., Dalton Trans.*, 2000, 745–751; (*e*) H. Schumann, P. R. Lee and J. Loebel, *Angew. Chem., Int. Ed. Engl.*, 1989, **28**, 1033–1035.

11 F. Franceschi, F. Hesschenbrouck, E. Solari, C. Floriani, N. Re, C. Rizzoli and A. Chiesi-Villa, *J. Chem. Soc., Dalton Trans.*, 2000, 593–604.

12 Because of the low quality of the crystal, the resulting determination of K-**3a** is poor (high residuals). Nevertheless, the structure is included here since it confirms unambiguously the connectivity of the molecule.

13 M. D. Ward, J. S. Fleming, E. Psillakis, J. C. Jeffery and J. A. McCleverty, *Acta Crystallogr., Sect. C: Cryst. Struct. Commun.*, 1998, **54**, 609–612.

14 Coordinated water should come from the presence of adventitious water in the solvents. All the attempts to crystallize Li-**3a** without it were unsuccessful.

15 See for example: (*a*) D. W. Lee and K. M. Ok, *Inorg. Chem.*, 2013, **52**, 5176–5184; (*b*) L. Balloch, A. M. Drummond, P. García-Álvarez, D. V. Graham, A. R. Kennedy, J. Klett, R. E. Mulvey, C. T. O'Hara, P. J. A. Rodger and I. D. Rushworth, *Inorg. Chem.*, 2009, **48**, 6934–6944; (*c*) W. J. Evans, D. B. Rego and J. W. Ziller, *Inorg. Chem.*, 2006, **45**, 3437–3443; (*d*) M. N. S. Hill, K. Izod, P. O'Shaughnessy and W. Clegg, *Organometallics*, 2000, **19**, 4531–4535.

16 M. Tsutsui, C. P. Hrung, D. Ostfeld, T. S. Srivastava, D. L. Cullen and E. F. Meyer, *J. Am. Chem. Soc.*, 1975, **97**, 3952–3965.

17 As shown in the Experimental section, complexes **3a** are indistinctly obtained either by treating *fac*-[$Mn(CO)_3Br(NCMe)_2$] with two equivalents of pyridylpyrazolate or by treating **1a** with an extra equivalent of pyridylpyrazole and two equivalents of a base.

18 Distances and angles of Mn(1) and Mn(2) are very similar. Table 3 collects only those for Mn(1). Complete tables can be found in the CIF.

19 See for example: (*a*) K. R. Reddy and M. V. Rajasekharan, *Polyhedron*, 1994, **13**, 765–769; (*b*) T. J. Malinowski, V. C. Kravtsov, Y. A. Simonov, J. Lipkowski and O. A. Bologa, *J. Coord. Chem.*, 1996, **37**, 187–193; (*c*) S. McCann, M. McCann, M. T. Casey, M. Jackman, M. Devereux and V. McKee, *Inorg. Chim. Acta*, 1998, **279**, 24–29; (*d*) D. A. Edwards, G. M. Hoskins, M. F. Mahon, K. C. Molloy and G. R. G. Rudolph, *Polyhedron*, 1998, **17**, 2321–2326; (*e*) Y. Yamamoto, T. Suzuki and S. Kaizaki, *J. Chem. Soc., Dalton Trans.*, 2001, 1566–1572; (*f*) Z. Li, D. Xu, J. Nie, Z. Wu, J. Wu and M. Y. Chiang, *J. Coord. Chem.*, 2002, **55**, 1155–1160; (*g*) J.-Z. Wu, E. Bouwman, A. M. Mills, A. L. Spek and J. Reedijk, *Inorg. Chim. Acta*, 2004, **357**, 2694–2702; (*h*) L. F. Jones, K. D. Camm, C. A. Kilner and M. A. Halcrow, *CrystEngComm*, 2006, **8**, 719–728; (*i*) L. Xiao, S. Jie, Y. Song, X. Cao and W. H. Sun, *J. Organomet. Chem.*, 2008, **693**, 3858–4866; (*j*) J. Rich, M. Rodríguez, I. Romero, L. Vaquer, X. Sala, A. Llobet, M. Corbella, M.-N. Collomb and X. Fontrodona, *Dalton Trans.*, 2009, 8117–8126; (*k*) C. M. Coates, A.-G. D. Nelson and C. R. Goldsmith, *Inorg. Chim. Acta*, 2009, **362**, 4797–4803; (*l*) A. Lennartson, *J. Coord. Chem.*, 2010, **63**, 4177–4187; (*m*) A. S. Roy, M. K. Biswas, T. Weyhermuller and P. Ghosh, *Dalton Trans.*, 2011, **40**, 146–155.

20 S. Dehghanpour and R. Aleesha, *Synth. React. Inorg., Met.-Org., Nano-Met. Chem.*, 2012, **42**, 1132–1138.

21 C. B. Anderson, A. B. S. Elliot, C. J. McAdam, K. C. Gordon and J. D. Crowley, *Organometallics*, 2013, **32**, 788–797.

22 S. Dehghanpour, J. Lipkowski, A. Mahmoudi and M. J. Khalaj, *Coord. Chem.*, 2010, **63**, 1473–1479.

23 (*a*) M. S. Jana, A. K. Pramanik, S. Kundu and T. K. Mondal, *Polyhedron*, 2012, **40**, 46–52; (*b*) M. S. Jana, A. K. Pramanik, S. Kundu, D. Sarkar and T. K. Mondal, *Inorg. Chim. Acta*, 2013, **399**, 138–145.

24 B. J. Liddle, S. Wanniariachchi, S. V. Lindeman and J. R. Gardinier, *J. Organomet. Chem.*, 2010, **695**, 53–61.

25 (*a*) M. F. C. Guedes da Silva and A. J. L. Pombeiro, *Electrochim. Acta*, 2012, **82**, 478–483; (*b*) A. J. L. Pombeiro, *Eur. J. Inorg. Chem.*, 2007, 1473–1482; (*c*) A. J. L. Pombeiro, *J. Organomet. Chem.*, 2005, **690**, 6021–6040; (*d*) A. B. P. Lever, *Inorg. Chem.*, 1991, **30**, 1980–1985; (*e*) A. B. P. Lever, *Inorg. Chem.*, 1990, **29**, 1271–1285; (*f*) http://www.chem.yorku.ca/profs/lever/elparameter98.htm

26 D. D. Perrin and W. L. F. Armarego, *Purification of Laboratory Chemicals*, Pergamon Press, Oxford, 3rd edn, 1988.

27 M. F. Farona and K. F. Kraus, *Inorg. Chem.*, 1970, **9**, 1700–1704.

28 (*a*) A. J. Amoroso, A. M. C. Thompson, J. C. Jeffery, P. L. Jones, J. A. McCleverty and M. D. Ward, *J. Chem. Soc., Chem. Commun.*, 1994, 2751–2752; (*b*) H. Brunner and T. Scheck, *Chem. Ber.*, 1992, **125**, 701–709.

29 *SAINT+. SAX area detector integration program. Version 6.02*, Bruker AXS, Inc., Madison, WI, 1999.

30 (*a*) G. M. Sheldrick, *SHELXTL, An integrated system for solving, refining, and displaying crystal structures from diffraction data. Version 5.1*, Bruker AXS, Inc., Madison, WI, 1998; (*b*) G. M. Sheldrick, *Acta Crystallogr., Sect. A: Fundam. Crystallogr.*, 2008, **64**, 112–122.

31 G. M. Sheldrick, *SADABS, Empirical Absorption Correction Program*, University of Göttingen, Göttingen, Germany, 1997.

32 (*a*) M. Nardelli, *Comput. Chem.*, 1983, **7**, 95–98; (*b*) M. Nardelli, *J. Appl. Crystallogr.*, 1995, **28**, 659.

33 (*a*) G. A. Jeffrey and L. Lewis, *Carbohydr. Res.*, 1978, **60**, 179–182; (*b*) R. Taylor and O. Kennard, *Acta Crystallogr., Sect. B: Struct. Sci.*, 1983, **39**, 133–138.

34 (*a*) A. J. L. Pombeiro, M. F. C. G. Silva and M. A. N. D. A. Lemos, *Coord. Chem. Rev.*, 2001, **219**, 53–80; (*b*) M. E. N. P. R. A. Silva, A. J. L. Pombeiro, J. J. R. F. da Silva, R. Herrmann, N. Deus, T. J. Castilho and M. F. C. G. Silva, *J. Organomet. Chem.*, 1991, **421**, 75–90.